Journal of Magnetics 10(3), 128-132 (2005)

Optical Properties of Two Different Metallic Na_xCoO_2: $x = 0.35$ and 0.75

J. Hwang[1]*, J. Yang[2], T. Timusk[1,2], and F. C. Chou[3]

[1]*Department of Physics and Astronomy, McMaster University, Hamilton, Ontario L8S 4M1, Canada*
[2]*The Canadian Institute of Advanced Research, Toronto, Ontario M5G 1Z8, Canada*
[3]*Center for Materials Science and Engineering, MIT, Cambridge, Massachusetts 02139, USA*

(Received 28 July 2005)

We report optical ab-plane properties of the layered sodium cobaltate, Na_xCoO_2 for $x = 0.35$ and 0.75. Two samples show metallic behaviors according to dc resistivity transport. Overall temperature dependent optical conductivities of both samples are very similar to those of the high temperature superconducting underdoped cuprates. We found that the optical scattering rate of $x = 0.75$ sample, which is in a Curie-Weiss metallic phase, varies linearly (non-Fermi liquid) with frequency and temperature while that of $x = 0.35$ sample, which is in a paramagnetic metallic phase, varies quadratically (Fermi liquid) with frequency and temperature. Both $x = 0.35$ and 0.75 samples have an onset of scattering around 600 cm^{-1} which can be attributed to the interaction of charge carriers with a bosonic collective mode in a system.

Key words : Sodium cobaltate, Optical conductivity, Optical scattering rate, Bosonic collective mode

1. Introduction

Since the recently discovery of the superconductivity in water intercalated sodium cobalt oxide, $Na_xCoO_2yH_2O$ ($1/4 < x < 1/3$ and $y = 1.4$) [1-4] the material has been studied intensively. The sodium cobalt oxide or sodium cobaltate, Na_xCoO_2, has a layered crystal structure; CoO_2 layer consists of tilled octahedral CoO_6, which makes cobalt layer sandwiched by two oxygen layers, and sodium layer is between CoO_2 layers. All layers are triangular lattices. The Co^{4+} (Co^{3+}) ion has spin 1/2 (0) and sits on a triangular Co lattice and may give rise to novel quantum states [5, 6]. This system may be an ideal one for the Anderson's resonating valence bond (RVB) theory [7]. In many ways it is very similar to the famous high temperature superconducting copper oxides, cuprates. The Na_xCoO_2 material has a rich and unique phase diagram [8, 9] which is based on dc resistivity, magnetic susceptibility, and electron diffraction measurements. According to the phase diagram there is a charge ordered insulating phase at $x = 0.50$ which separates two different metallic phases; a paramagnetic for $x < 0.50$ and a Curie-Weiss for $x > 0.50$. In $x = 0.50$ sample, a superstructure observed in the Na layer by the electron diffraction study has been suggested that the insulating state is induced by this superstructure [9].

In this paper we focus on two different metallic phases in the phase diagram [9]. We used optical spectroscopy to study two different Na_xCoO_2 samples in two different sodium concentrations; $x = 0.35$ and 0.75 at various temperatures. We indeed observed two different metallic phases (Fermi liquid and non-Fermi liquid) at two different samples with $x = 0.35$ (Fermi) and 0.75 (non-Fermi). The infrared reflectance at room temperature is very similar to that of the underdoped cuprates with the reflectance decreasing roughly linearly with frequency over a broad region extending to nearly 0.75 eV (see Figure 1). As the temperature is lowered below ambient temperature both samples show a shoulder-like (step-like) feature develops in the reflectance (the optical scattering rate) near 600 cm^{-1} (see Figure 1 and 4), characteristic of the interaction of the charge carriers with a bosonic collective mode [10-12] in the system.

2. Experments and Data Analysis

We grew the parent single crystals ($x = 0.75$) by the floating zone method and removed sodium atom to control Na concentration by the electrochemical method [3]. We determined the Na concentration by the electron

*Corresponding author: Tel: +1-905-525-9140 Ext. 22016, Fax: +1-905-546-1252, e-mail: hwangjs@mcmaster.ca

© 2005 Journal of Magnetics

probe microanalysis (EPMA) and we estimate the uncertainty in x to be $\leq\pm$ 0.05. We took optical data of freshly cleaved ab-plane surface of 2×2 mm^2 crystals in a ^{4}He flow cryostat. We measured the ab-plane reflectance between 50 and 40,000 cm^{-1} using an *in situ* gold evaporation method [13] and a commercial Fourier transform infrared (FTIR) spectrometer, Bruker 66 v/S. We also used an advanced measurement technique, which is called an automated temperature dependent reflectance measurement technique [14]. We estimate the absolute accuracy of the reflectance to be better than 0.5%.

Figure 1(a) and (b) show the raw reflectance data of our two samples: $x = 0.35$ and 0.75. At room temperature, reflectance of both samples show near linear dependence with respect to frequency up to high frequencies; 6000 cm^{-1} for 0.35 sample and 3000 cm^{-1} for 0.75 sample. As lowering temperatures we observe that at high frequency range there is no temperature dependence and at low frequency range there is strong temperature dependence and a shoulder-like feature appears below 600 cm^{-1} for both of the samples. These room and low temperature properties are very similar to those of underdoped cuprates [15, 16].

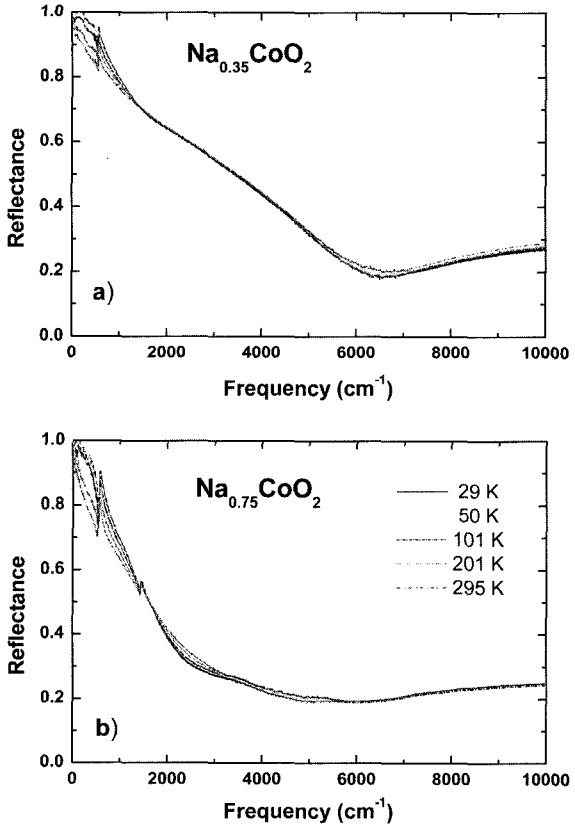

Fig. 1. (a) Measured reflectance of the $x = 0.35$ sample at five different temperatures. (b) Measured reflectance of the $x = 0.75$ sample at five different temperatures.

Reflectance is easily measured but the quantity itself is a complicated optical quantity to be explained. So we need to extract some easier optical quantities to explain, which are optical constants; optical conductivity, dielectric constants, and so on.

3. Optical Conductivity and Scattering Rate

To extract optical constants from measured reflectance, $R(\omega)$, in finite spectral range the first step will be a Kramers-Kronig (KK) transformation [17]:

$$\phi(\omega) = -\frac{1}{2\pi}\int_0^\infty \ln\left|\frac{s+\omega}{s-\omega}\right|\frac{d\ln R(s)}{ds}ds \tag{1}$$

where $R(\omega)$ and $\phi(\omega)$ are the reflectance and the phase, respectively. For performing KK transformation we used the measured dc resistivity to extend the data to zero frequency for the $x = 0.75$ sample. For the $x = 0.35$ sample we used the Hagen-Rubens frequency dependence for $\omega \rightarrow 0$ extrapolation, $1 - R(\omega) \propto \omega^{1/2}$. At high frequencies we used the data of Caimi *et al.* [18] between 40 000 and 100 000 cm^{-1} and extrapolations assuming a free carrier response beyond 100 000 cm^{-1}, $R(\omega) \propto \omega^{-4}$.

To extract further optical constants we used Fresnel's equation for normal incident case as an approximation:

$$\frac{1-n(\omega)-ik(\omega)}{1+n(\omega)+ik(\omega)} = \sqrt{R(\omega)e^{i\phi(\omega)}} \tag{2}$$

where $n(\omega)$ and $k(\omega)$ are the index of refraction and the extinction coefficient, respectively. We also used relationships between optical constants [17]:

$$\varepsilon_1(\omega) = n^2(\omega) - k^2(\omega) \tag{3}$$
$$\varepsilon_2(\omega) = 2n(\omega)k(\omega)$$

and

$$\sigma(\omega) \equiv \sigma_1(\omega) + i\sigma_2(\omega) = -i\frac{\omega}{4\pi}[(\varepsilon_1(\omega) - \varepsilon_H) + i\varepsilon_2(\omega)] \tag{4}$$

where $\varepsilon_1(\omega)$ and $\varepsilon_2(\omega)$ are the optical dielectric constants and $\sigma(\omega) \equiv \sigma_1(\omega) + i\sigma_2(\omega)$ is the complex optical conductivity. ε_H is the dielectric constant of the background ions. We take ε_H as $\varepsilon_1(\omega)$ at a high frequency (~1.5 eV). In principle we can extract any other optical constants using other relationships between optical constants [17].

Figure 2(a) and (b) show the real part of the optical conductivity, $\sigma_1(\omega)$, of our two samples at five different temperatures. The optical conductivity is a frequency dependent conductivity or current in a system. At room temperature we observe a broad band below 7000 cm^{-1},

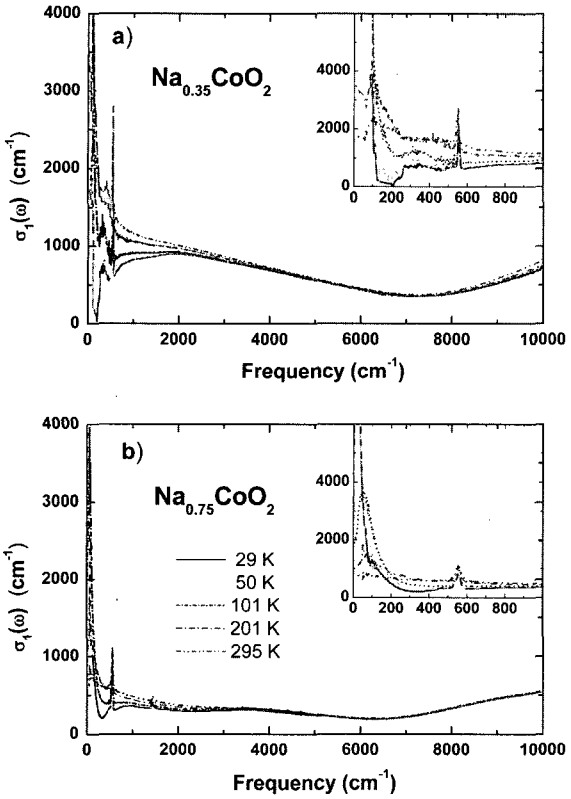

Fig. 2. (a) The real part of the optical conductivity of the $x = 0.35$ sample extracted from reflectance at five different temperatures. In the inset we show a magnified figure at low frequency range. (b) The real part of the optical conductivity of the $x = 0.75$ sample extracted from reflectance at five different temperatures. In the inset we show a magnified figure at low frequency range.

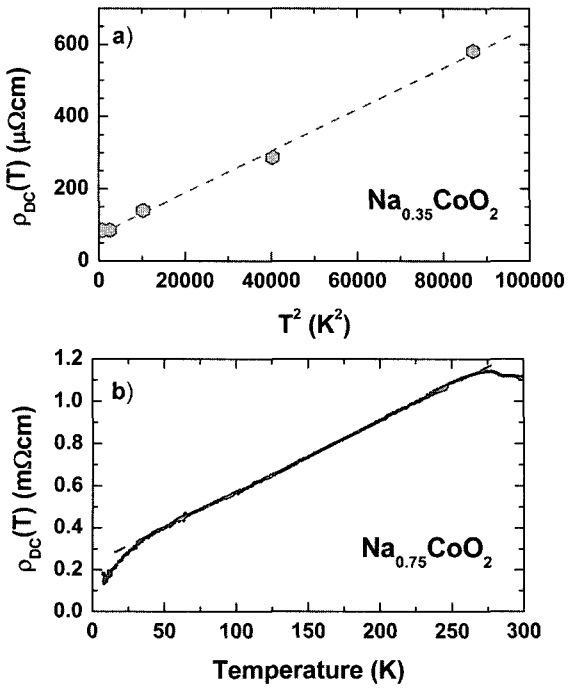

Fig. 3. (a) Extracted dc resistivity from an extrapolation to zero frequency of the optical conductivity as a function of w^2. The dashed line is a linear fit to the data. (b) Measured dc resistivity of the $x = 0.75$ sample. The dashed line is a linear fit to the data between 30 K and 270 K.

which is a combination of the Drude band and a mid-infrared band. As lowering temperature we are able to see the separation between the two bands with a deep valley near 400 cm^{-1}. These properties are similar to those of underdoped cuprates [19]. The sharp peak near 550 cm^{-1} is a phonon mode in the system [20].

We define the effective number of charge carriers per copper atom in terms of the partial sum rule as the following equation:

$$N_{eff}(\omega) = \frac{2mV_{Cu}}{\pi e^2}\int_{0^+}^{\omega}\sigma_1(\omega')d\omega'$$

where ω is a cutoff frequency, m is the free electron mass and V_{Cu} is the volume per copper atom, 57.7 Å^3. The Drude spectral weight, which is N_{eff} at the cutoff frequency, 7500 cm^{-1}, of the $x = 0.35$ sample is consistent with the doping dependent spectral weight in our previous study [21]; N_{eff}(7500 cm^{-1}) = 0.114 holes/Cu.

Figure 3(a) shows a dc resistivity extracted from the optical conductivity of the $x = 0.35$ sample by extrapolation to zero frequency. The extracted dc resistivity has a quadratic function of temperature. The dc resistivity is quadratically dependent of temperature; $\rho_{DC}(T) \propto T^2$. Figure 3(b) shows a measured dc resistivity of the $x = 0.75$ sample. We have three interesting features in the measured dc resistivity [22]; Na ordering temperature near $T = 280$ K, antiferromagnetic ordering below 28 K (Neel temperature), and a linear temperature dependence between the two characteristic temperatures; $\rho_{DC}(T) \propto T$. Both $x = 0.35$ and 0.75 samples show metallic behavior.

The extended Drude model offers a detailed view of the charge carrier scattering spectrum and its contribution to the effective mass [11, 12, 23, 24]. In this picture the scattering rate in the Drude expression is allowed to have frequency dependence:

$$\sigma(\omega) = \frac{i}{4\pi}\frac{\omega_p^2}{\omega + [\omega\lambda(\omega) + i1/\tau(\omega)]} \quad (5)$$

where ω_p is the plasma frequency, $1/t(\omega)$ is the scattering rate and $\lambda(\omega)+1 = m^*(\omega)/m$, $m^*(\omega)$ is an effective mass and m is the bare mass.

Figure 4(a) and (b) show the optical scattering rates of the $x = 0.35$ and 0.75 samples, respectively. For the 0.75

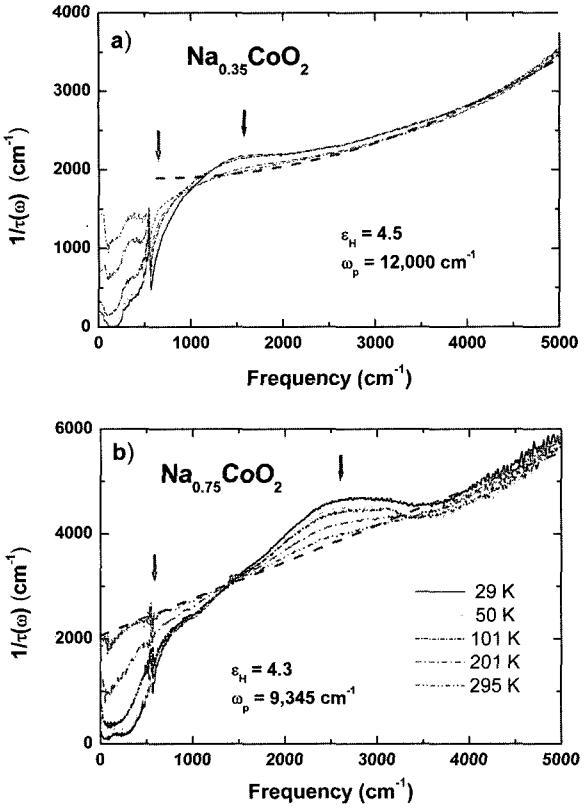

Fig. 4. (a) The optical scattering rate of the x = 0.35 sample, which is extracted by using Eq. (5). The dashed line is a quadratic curve fit to the room temperature data between 1000 cm^{-1} and 5000 cm^{-1}. (b) The optical scattering rate of the x = 0.75 sample, which is extracted by using Eq. (5). The dashed line is a linear fit to the room temperature data between 500 cm^{-1} and 5000 cm^{-1}.

sample we removed the phonon mode near 550 cm^{-1}. Both scattering rates show two common features; one is a step-like feature or onset of scattering near 600 cm^{-1} and the other is a hump-like feature at low temperature. The onset scattering has been attributed to an interaction of charges carriers with a bosonic collective mode or magnetic resonance mode in the system [11, 12, 23]. We can expect that these two systems may have a collective bosonic mode or a magnetic resonance mode. The hump-like feature needs to be explained. Differences between scattering rates of the x = 0.35 and 0.75 are the center frequencies of the hump-like feature; ~1700 cm^{-1} for the 0.35 sample and ~2700 cm^{-1} for the 0.75 sample.

From observation of Figure 3 and 4 we are be able to see temperature and frequency dependencies of the scattering rates; $1/\tau(\omega, T) \sim a\omega^2 + bT^2$ (Fermi liquid behavior) for the 0.35 sample and $1/\tau(\omega, T) \sim a'\omega + b'T$ (non-Fermi liquid behavior) for the 0.75 sample, here a, b, a' and b' are constants.

4. Conclusions

In conclusion we studied sodium cobaltates in two different metallic samples using optical spectroscopy. Two metallic samples (x = 0.35 and 0.75) have a bosonic collective mode, which interact with charge carriers in the system and causes a strong onset scattering around 600 cm^{-1}. The x = 0.35 sample, which is a paramagnetic metal in the phase diagram, shows Fermi liquid behavior, while the x = 0.75 sample, which is a Curie-Weiss metal in the phase diagram, shows non-Fermi liquid behavior. This difference may be the fundamental one between two different metallic phases in the phase diagram.

References

[1] K. Takada, H. Sakurai, E. Takayama-Muromachi, F. Izumi, R. A. Dilanian, and T. Sasaki, Nature (London) **422**, 453 (2003).
[2] R. E. Schaak, T. Klimczuk, M. L. Foo, and R. J. Cava, Nature (London) **424**, 527 (2003).
[3] F. C. Chou, J. H. Cho, P. A. Lee, E. T. Abel, K. Matan, and Y. S. Lee, Phys. Rev. Lett. **92**, 157004 (2004).
[4] R. Jin, B. C. Sales, P. Khalifah, and D. Mandrus, Phys. Rev. Lett. **91**, 217001 (2003).
[5] G. Baskaran, Phys. Rev. Lett. **91**, 097003 (2003).
[6] Q. H. Wang, D. H. Lee, and P. A. Lee, Phys. Rev. B **69**, 092504 (2004).
[7] P. W. Anderson, Science **235**, 1196 (1987).
[8] R. Ray, A. Ghoshray, K. Ghoshray, and S. Nakamura, Phys. Rev. B **59**, 9454 (1999).
[9] M. L. Foo, Y. Wang, S. Watauchi, H. W. Zandbergen, T. He, R. J. Cava, and N. P. Ong, Phys. Rev. Lett. **92**, 247001 (2004).
[10] J. P. Carbotte, E. Schachinger, and D. N. Basov, Nature (London) **401**, 354 (1999).
[11] J. Hwang, T. Timusk, and G. D. Gu, Nature (London) **427**, 714 (2004).
[12] J. Hwang, J. Yang, T. Timusk, S. G. Sharapov, J. P. Carbotte, D. A. Bonn, R. Liang, and W. Hardy, cond-mat/0505302 (2005).
[13] C. C. Homes, M. A. Reedyk, D. A. Crandles, and T. Timusk, Appl. Opt. **32**, 2976 (1993).
[14] J. Hwang and T. Timusk (unpublished).
[15] J. Hwang, T. Timusk, A. V. Puchkov, N. L. Wang, G. D. Gu, C. C. Homes, J. J. Tu, and H. Eisaki, Phys. Rev. B **69**, 094520 (2004).
[16] Z. Schlezinger, R. T. Collins, F. Holtzberg, C. Feild, S. H. Blanton, U. Welp, G. N. Crabtree, Y. Fang, and J. Z. Liu, Phys. Rev. Lett. **65**, 801 (1990).
[17] Frederick Wooten, Optical Properties of Solids, Academic, New York (1972).
[18] G. Caimi, L. Degiorgi, H. Berger, N. Barisic, L. Forro, and F. Bussy, Euro. Phys. J. B **40** (3), 231 (2004).

[19] A. V. Puchkov, P. Fournier, D. N. Basov, T. Timusk, A. Kapitulnik, and N. N. Kolesnikov, Phys. Rev. Lett. **77**, 3212 (1996).
[20] N. L. Wang, P. Zheng, D. Wu, Y. C. Ma, T. Xiang, R. Y. Jin, and D. Mandrus, Phys. Rev. Lett. **93**, 237007 (2004).
[21] J. Hwang, J. Yang, T. Timusk, and F. C. Chou, will be appeared in Phys. Rev. B **72**(1), (2005).
[22] J. Wooldridge, D. McK Paul, G. Balakrishnan, and M. R. Lees, cond-mat/0406513 (2004).
[23] P. B. Allen, Phys. Rev. B **3**, 305 (1971).
[24] A. V. Puchkov, D. N. Basov, and T. Timusk, J. Physics, Condensed Matter **8**, 10049 (1996).